Cent. Eur. J. Chem. • 7(4) • 2009 • 809–817
DOI: 10.2478/s11532-009-0083-2

VERSITA

Central European Journal of **Chemistry**

High surface area nano-sized $La_{0.6}Ca_{0.4}MnO_3$ perovskite powder prepared by low temperature pyrolysis of a modified citrate gel

Research Article

Meysam Soleymani[1], Ahmad Moheb[1,*], Ezatolah Joudaki[2]

[1]*Department of Chemical Engineering, Isfahan University of Technology, Isfahan 84156-83111, Iran*

[2]*Chemical Engineering Group, Faculty of Engineering, Arak University, Arak 38139, Iran*

Received 31 December 2008; Accepted 7 May 2009

Abstract: Single phase nanocrystalline $La_{0.6}Ca_{0.4}MnO_3$ powder was synthesized by both the usual and a modified citrate gel precursor method, and the effects on the formation of homogeneous nano-sized powder with a perovskite structure were investigated. In the modified method, single phase $La_{0.6}Ca_{0.4}MnO_3$ powder with an average particle size of 17.2 nm was obtained when the powder was pyrolyzed at 520°C for 2 h. Its specific surface area was 40.7 $m^2\ g^{-1}$, about 4-fold larger than that of powder made by the usual citrate gel method.

Keywords: *$La_{0.6}Ca_{0.4}MnO_3$ • Sol-gel Method • Nano-sized Powder • High Surface Area • Perovskite*

1. Introduction

The properties of perovskite oxides with the general formula of ABO_3 can vary over a wide range depending on A and B, as the cubic perovskite lattice is a rather rugged host for a variety of mixed transition metal oxides. Substituted perovskite can generally be described by the formula $A_{1-x}A'_xB_{1-y}B'_yO_3$. Extensive research has focused on several catalytic applications [1-4]. Manganese-containing perovskites have received great attention due to their high catalytic activity for destruction of common exhaust pollutants such as CO, hydrocarbons and nitrogen oxides [5-9]. La-based perovskites ($La_{1-x}A'_xMnO_3$, A'= Ca or Sr) also have shown electro-catalytic activity for oxygen reduction (very important in fuel cells) [10,11], the chlor-alkali electrolysis process and air batteries [10-13]. Therefore, synthesis of homogenous nanocrystalline $La_{1-x}A'_xMnO_3$ (A'= Ca or Sr) with high surface area and powders without any impurity phase is very important.

Perovskites usually possess a very low specific surface area (SSA), generally <2 $m^2\ g^{-1}$; consequently the low specific catalytic activity greatly limits practical application [14,15]. Increasing the SSA requires lowering the calcination temperature, demanding that the precursor elements be uniformly dispersed at the molecular level to speed the solid-state reaction. Several syntheses have been developed based on this hypothesis: (1) spray-freezing/freeze-drying [16], in which the minimum temperature and time necessary for obtaining a single perovskite phase are about 500°C and 15 h, with the product SSA in the range 8–22 $m^2\ g^{-1}$ and requiring complicated equipment; (2) cyanide decomposition [17] giving SSA exceeding 30 $m^2\ g^{-1}$ (although cyanides are toxic); and (3) complexation with an organic ligand such as citrate in

* *E-mail: Ahmad@cc.iut.ac.ir*

synthesizing $LaCoO_3$ or $LaMnO_3$ [18]. The minimum calcination temperature and time for obtaining a single perovskite phase are 700˚C and 4h, and product SSA can exceed 10 $m^2 g^{-1}$ [19].

The focus of the present work was modification of the citrate gel precursor method for synthesis of $La_{0.6}Ca_{0.4}MnO_3$ perovskite to give a higher SSA. Precursor elements were more uniformly dispersed at the molecular level and the $La_{0.6}Ca_{0.4}MnO_3$ perovskite synthesized was characterized by several techniques. Its properties were compared with those of the oxide synthesized by the usual citrate gel precursor method.

2. Experimental Procedures

2.1. Synthesis of La-Ca-Mn-citrate precursor

$La_{0.6}Ca_{0.4}MnO_3$ powders were synthesized by the citrate gel precursor method [20]. For the preparation of the precursor solution, calcium nitrate (Merck), manganese nitrate (Merck), lanthanum nitrate (Aldrich), citric acid (Merck) and aqueous ammonia (Merck) were used. The metal nitrates were weighed according to the nominal $La_{0.6}Ca_{0.4}MnO_3$ composition and dissolved in deionized water. This solution was slowly dropped into a citric acid solution with a citric acid: total metal mole ratio of 1.2:1.0. The homogeneous solution obtained after mixing (pH≈1) was slowly evaporated on a water bath at 75-80˚C to a viscous gel. This gel was dried in an oven, slowly increasing the temperature to 120-130˚C and maintaining this temperature overnight to produce a solid amorphous citrate precursor. In some cases, the pH of the mixed solution was adjusted to 8-9 by adding aqueous ammonia. The dried gels obtained at pH 1 and 8-9 were labeled as P_L and P_H, respectively.

2.2. Preparation of $La_{0.6}Ca_{0.4}MnO_3$ powder

The $La_{0.6}Ca_{0.4}MnO_3$ was prepared by pyrolyzing the precursor in a furnace in air. The temperature was first slowly raised to 300˚C (5-10˚C min^{-1}) and held for 30 minutes to decompose the organic components. It was then increased to various pre-set temperatures and held for a definite time to form the perovskite oxide.

2.3. Powder characterization

2.3.1. Thermogravimetry and differential thermal analysis

Thermogravimetry and differential thermal analysis (TG/DTA) curves in air were simultaneously obtained using a Perkin-Elmer Diamond TG/DTA instrument. The sample and reference were placed in platinum crucibles, and α-Al_2O_3 was the inert reference. The results were recorded from room temperature to 700˚C; the temperature was held at 700˚C for 2 h then increased to 900˚C, with a 5˚ C min^{-1} ramp in all steps.

2.3.2. IR spectroscopy

IR spectroscopy of pressed KBr pellets was carried out on a JASCO FTIR 680-Plus Spectrometer in the region 4000–400 cm^{-1}.

2.3.3. X-ray diffraction

Phase purity and crystallinity of the calcined samples were characterized by powder X-ray diffraction (Philips, X-pert) with CuKα radiation using a Ni filter (λ=0.15418 nm). The data were collected at 0.05˚ steps for 5 sec per step over 2θ from 20 to 80˚.

2.3.4. Scanning electron microscopy

The morphology of the calcined powder was observed by scanning electron microscopy (SEM) of gold-sputtered samples using a Philips XL30 ESEM microscope operating in high vacuum at 10 kV.

2.3.5. Specific surface area measurements

Specific surface area (SSA) was measured by Brunauer-Emmett-Teller (BET) nitrogen adsorption-desorption [21] using a Chembet 3000.

3. Results and Discussion

There are four main factors affecting the formation of the gel as well as the calcined powder crystallinity and morphology. These are: mole ratio of citric acid to total metal cations content (Z=citric acid/ (La+Ca+Mn)), precursor solution pH, calcination temperature, and time.

The amount of citric acid used is important in precursor homogeneity. To prevent precipitation during dehydration and to maintain metal ion homogeneity on a molecular scale, the citric acid to metal ion molar ratio of should be sufficient [22]. Therefore, the effect of this ratio was investigated. Maintaining the metal ions in homogeneous solution during drying with Z<1.1 was difficult; insufficient citric acid can cause precipitation. When Z=1.1 no visible precipitation was observed during dehydration. For Z>2, large amounts of white crystals appeared, probably due to crystallization of excess citric acid. A homogeneous and transparent sol and gel can be produced with Z in the range of 1.1–2.0.

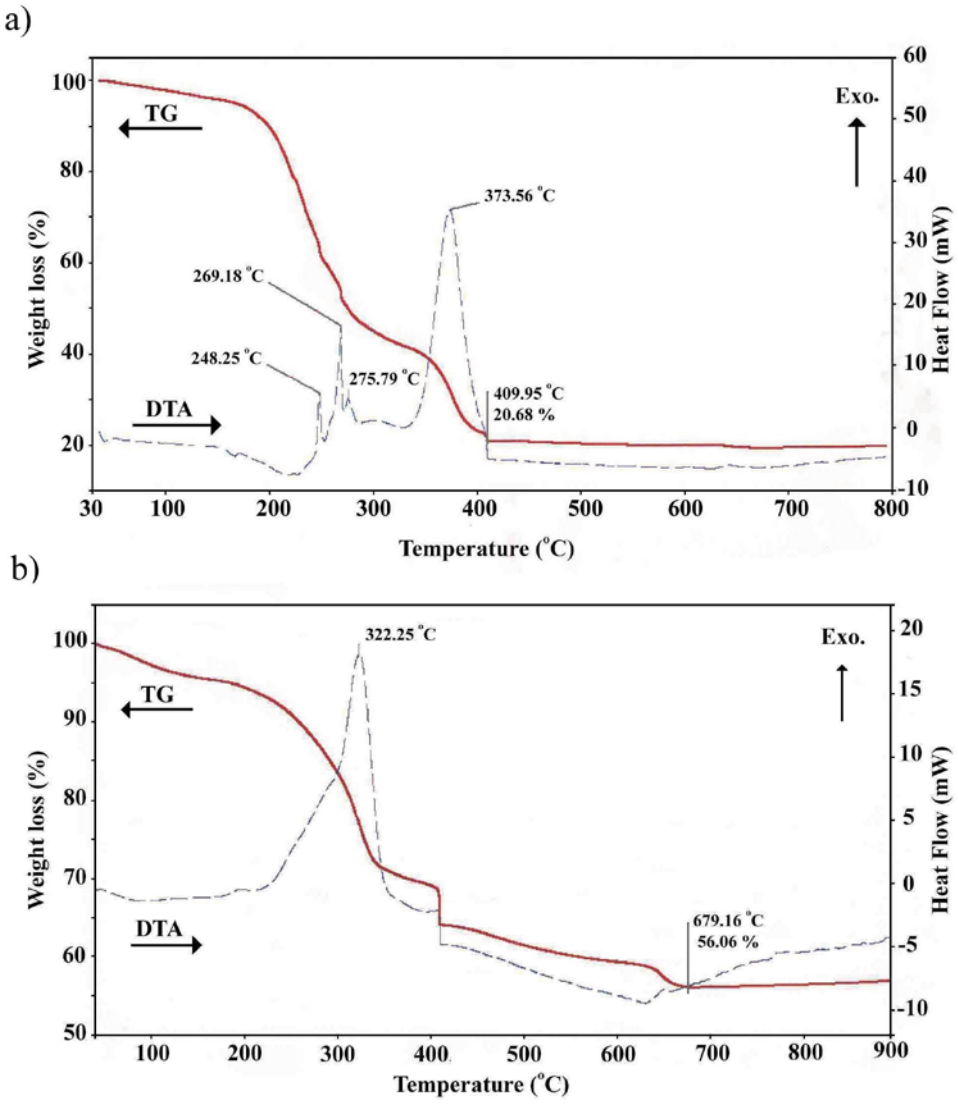

Figure 1. TG and DTA cures of citrate precursors, a) P_h and b) P_l.

3.1. Thermogravimetric and differential thermal analysis

Fig. 1a shows the thermogravimetric (TG) and differential thermal analysis (DTA) curves of the dried high pH citrate gel (P_H) used to estimate the calcination temperature. The TG curve shows weight loss in several steps, indicating that thermal decomposition occurred gradually. The first small weight loss of 6.6% below 180˚C is mostly due to dehydration and evaporation of volatile organic components. In the range of 180-300˚C the three successive exothermic peaks at 248.25, 269.18 and 275.79˚C, accompanied by a three-step weight loss of 48.4%, are assigned to decomposition of the citrate complex. The weight loss of about 25.0% in the range 300-410˚C is probably due to combustion of the remaining organic species, corresponding to the largest DTA exotherm at 373.56˚C. A very small weight loss which corresponds to a small DTA endotherm in the range of 410-550˚C was detected. It could be due to carbonate decomposition and perovskite formation [23]. No weight loss appeared thereafter.

For comparison, TG/DTA curves of the dried low pH citrate gel (P_L) are shown in Fig. 1b. Thermal decomposition varies with pH, and the final weight loss temperature for P_L is about 200˚C higher than for P_H. These results reveal that at high pH uniformity at the molecular scale is improved; hence $La_{0.6}Ca_{0.4}MnO_3$ can be obtained at a lower calcination temperature by decomposing an amorphous complex of La-Ca-Mn-citrate.

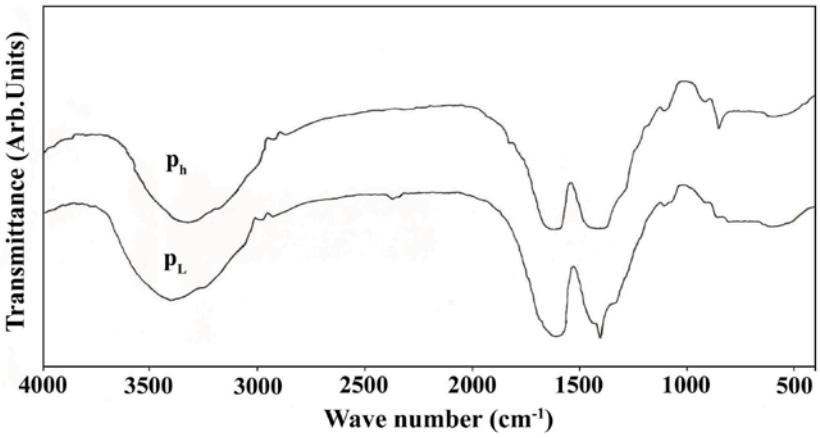

Figure 2. IR spectra of the dried gels P_l and P_h.

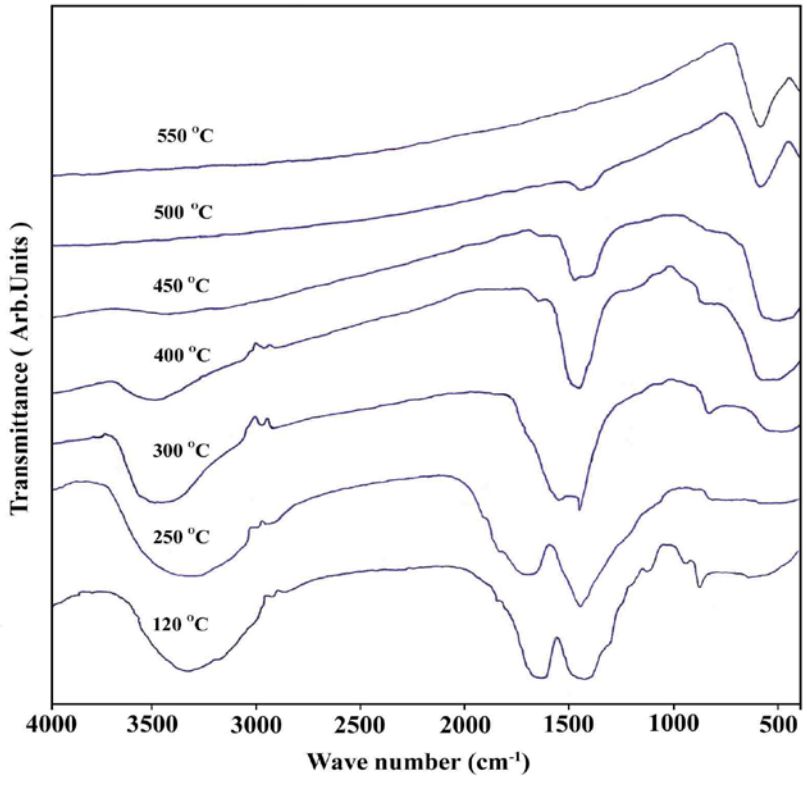

Figure 3. IR spectra of citrate precursor P_h calcined at various temperatures.

3.2. IR spectroscopy

The crystalline structure of the rare earth manganites is known to be of the distorted $GdFeO_3$-type structure in which a central Mn atom is octahedrally surrounded by six oxygen ions. The MnO_6 has nearly-ideal octahedral symmetry with six vibrational modes, but only two are IR active [24]. The band around 600 cm^{-1} corresponds to the stretching mode (v_s) of Mn—O—Mn or Mn—O bonds [25-27], while the bending mode (v_b) around 400 cm^{-1} is due to changes in the Mn—O—Mn bond angle.

Fig. 2 shows the IR spectra of the dried citrate gels P_L and P_H. For the dried gel P_L, the precursor gave somewhat complicated spectra. The absorption bands at 3400, 1600, 1410, 1385, 1270, and 1080 indicate the presence of citrate precursor. The very broad band at 3400 corresponds to a water stretch. Two strong bands at 1410 and 1600 cm^{-1} were assigned to the ionized carboxylate symmetric and asymmetric C—O stretching, though the latter band was superposed with a sharp 1385 cm^{-1} nitrate band. This means that the citric acid

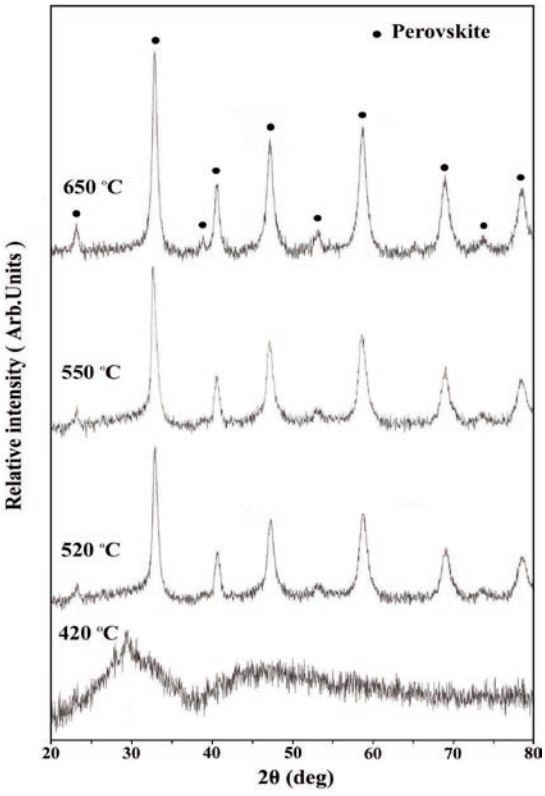

Figure 4. XRD of $La_{0.6}Ca_{0.4}MnO_3$ calcined at different temperatures.

carboxyl hydrogens were replaced by metal cations to form a citrate complex.

The IR spectra of the dried gel P_H and its calcination products are depicted in Fig. 3. In P_H the widened band at 1410 cm^{-1} indicates that metal cations are completely complexed by citric acid. When calcination temperature was increased to 400˚C the characteristic peak of complexed COO^- almost disappeared with a concomitant appearance of carbonate absorption at 860, 1060 and 1460 cm^{-1}. As the dried gel was calcined above 450˚C the 1460 cm^{-1} absorption peak decreased indicating carbonate decomposition, supported by the TG weight loss in the range of 410-550˚C. The wide 590 cm^{-1} absorption band of the gel calcined at 550˚C suggests perovskite formation.

3.3. X-ray diffraction

3.3.1. Calcination temperature

Powder pre-calcined from the dried citrate gel P_H at 300˚C was further calcined at temperatures from 450 to 650˚C for 2 h. Fig. 4 shows the XRD patterns at different stages of the heat treatment. The $La_{0.6}Ca_{0.4}MnO_3$ crystallinity strongly depends on calcination temperature. After calcination at 450˚C for 2 hours the XRD pattern showed no peaks, indicating that the sample was still amorphous. In contrast, when the precursor was calcined at 520˚C for 2 hours several sharp peaks were observed, attributed to the perovskite $La_{0.6}Ca_{0.4}MnO_3$ by comparison with standard XRD spectra. Thus, $La_{0.6}Ca_{0.4}MnO_3$ with a perovskite structure can be synthesized at 520˚C. There have been few reports of lower crystallization temperatures for the synthesis of such oxides. As also shown in Fig. 4, the perovskite peak grew stronger and sharper as the calcination temperature increased from 520 to 650˚C, indicating that the $La_{0.6}Ca_{0.4}MnO_3$ crystallinity improves with higher calcination temperature.

Fig. 5 shows the XRD patterns of the calcined powders derived from the precursor solutions with different pH values. The powders were calcined at 700˚C for 2 h. Single phase $La_{0.6}Ca_{0.4}MnO_3$ and unreacted materials co-existed when pH was 1. For high pH values (8-9) pure perovskite phase was obtained, suggesting incomplete metal complexation at low pH, probably due to incomplete citric acid dissociation.

3.3.2. Calcination time

Calcination time influences $La_{0.6}Ca_{0.4}MnO_3$ crystallization. As shown in Fig. 6, the XRD spectra of the powder calcined at 520˚C for 1 h exhibited not only $La_{0.6}Ca_{0.4}MnO_3$ diffraction peaks, but also some tiny peaks due to intermediates. They disappeared with

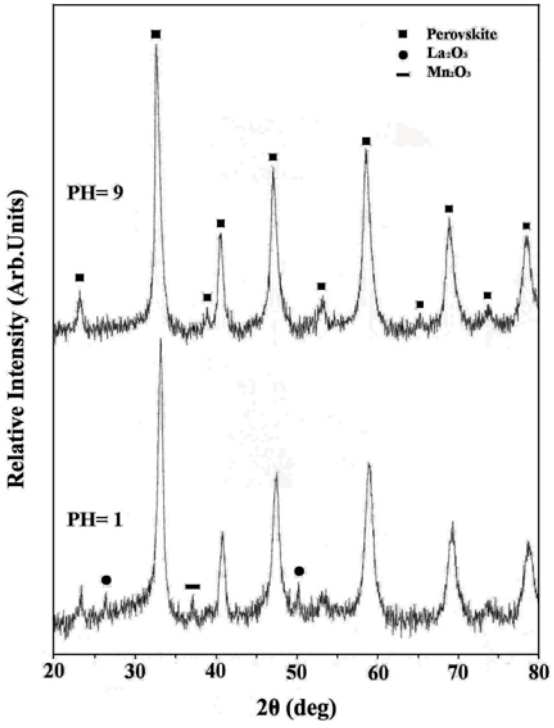

Figure 5. XRD of the powders derived from the precursor solutions with different pH values calcined at 700°C.

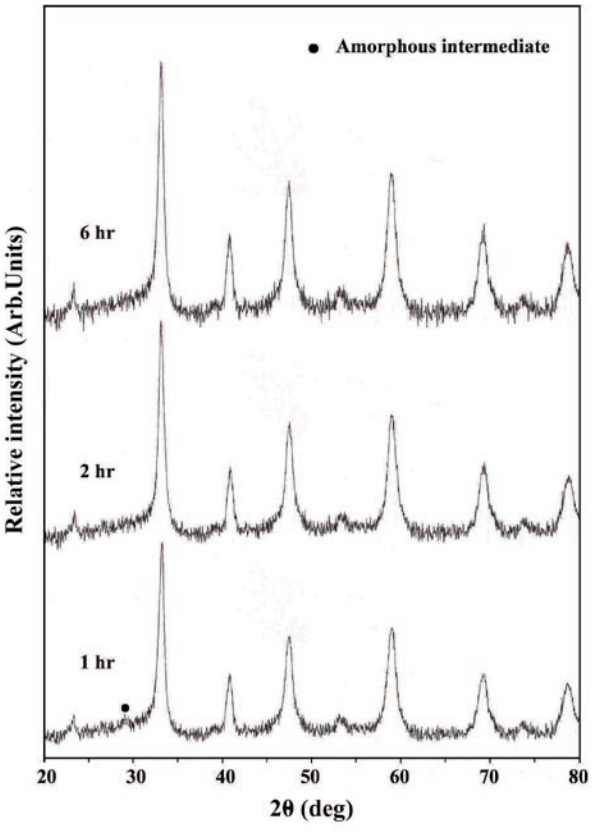

Figure 6. XRD of $La_{0.6}Ca_{0.4}MnO_3$ calcined at 520°C for various times.

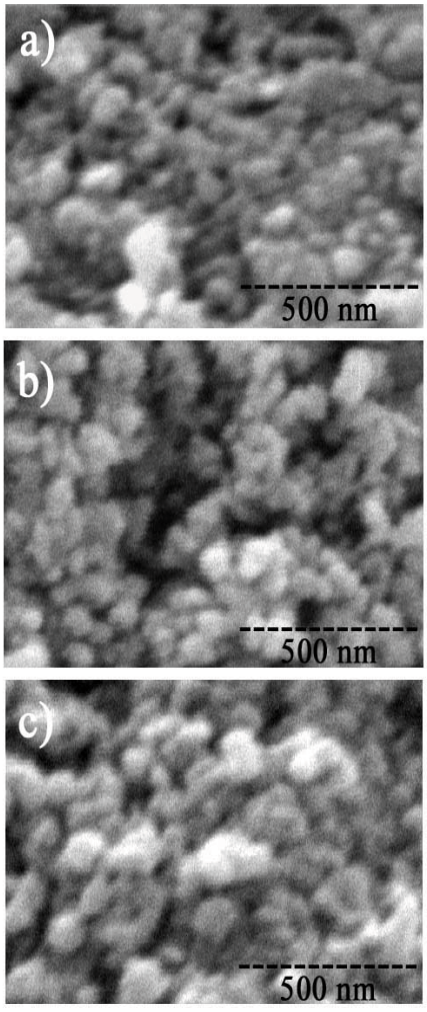

Figure 7. SEM images of $La_{0.6}Ca_{0.4}MnO_3$ powders prepared by the modified citrate gel precursor method and calcined at a) 520°C, b) 650°C and c) 750°C for 2 h.

the increase of calcination time to 2 h. The perovskite peak became only slightly sharper and stronger as the calcination increased from 2 to 6 h.

The average crystal size can be determined from the XRD pattern parameters according to Scherrer's formula ($D=0.89\lambda/B\cos\theta$), after Warren·s correction for instrumental broadening [28]. D is the particle diameter, λ is the wavelength (for Cu Kα, λ=1.5418 Å) and $B=(B_M^2-B_S^2)^{1/2}$ (B_M is the full width at half-maximum for the sample and B_S is that for a standard quartz). The results (Table 1) show calcination temperature is much more significant than calcination time.

3.4. Scanning electron microscopy

Scanning electron microscopy (SEM) of perovskite oxides prepared by the modified citrate gel method and calcined at various temperatures (520, 650 and 750˚C for 2 h) are shown in Fig. 7, and the particle sizes are in Table 1. Based on the SEM images, well-crystallized powders are synthesized with homogeneous morphology. The particles display regular shape with a narrow size distribution. The majority of the particles were distributed in the ranges 20-50, 60-100 or 80-120 nm for samples calcined at 520, 650 or 750˚C, respectively. Table 1 shows that the mean particle sizes obtained by SEM (D_{SEM}) are larger than those obtained by XRD peak broadening (D_{XRD}). Using these results it is possible to calculate the mean agglomeration degree (particle size/crystal size) for each sample. As can be seen in Table 1 the ratio of D_{SEM}/D_{XRD} becomes larger with increase of calcination temperature (2-2.6 for 520 and 550˚C and 3.6 at 750˚C). These results show that higher calcination temperature leads to formation of larger particles and their agglomeration.

The dependence of the average particle size on the heat-treatment time was also investigated (Table 1). The

Table 1. Dependence of particle size on calcination temperature and heat treatment time determined by SEM, XRD and BET.

Temperature (˚C)	D_{XRD} (nm)	D_{BET} (nm)	D_{SEM} (nm)	Agglomeration degree (D_{SEM}/D_{XRD})
520 (1 h)	17.2	22.3	20-50	2.0
520 (2 h)	17.2	23.3	20-50	2.0
520 (6 h)	18.4	24.5	30-50	2.2
550	19.3	25.9	40-60	2.6
650	23.7	35.7	60-100	3.3
750	27.5	43.8	80-120	3.6

Table 2. BET specific surface areas.

Sample	520 (˚C) - 1 h	520 (˚C) - 2 h	520 (˚C) - 6 h	550 (˚C) - 2 h	650 (˚C) - 2 h	750 (˚C) -2 h
SSA ($m^2\ g^{-1}$)	40.7	39.1	37.2	34.8	25.5	20.8

heat treatment time did not have a substantial effect. For example, samples calcined at 520˚C for 1 and 2 h had similar particle size and even increasing the time to 6 h did not cause a large difference.

3.5. BET specific surface area measurements

Table 2 shows the effects of calcination temperature and time on the specific surface areas (SSA). The specific surface area strongly decreased when calcination temperature increased from 520 to 750°C and it became smaller with increased calcination time. The larger the crystals the smaller the specific surface area is. On the basis of these observations, we are able to estimate from geometrical relationships ($D_{BET} = 6/(\rho \times S_{BET})$, where ρ is the theoretical density of $La_{0.6}Ca_{0.4}MnO_3$, based on Chen's study [29]) the particle size of the materials from the S_{BET} values, also presented in Table 1. The SSA of the powder from the modified citrate gel calcined at 520˚C was 40.7$m^2\ g^{-1}$, about 4-fold larger than that of the powder from the usual citrate gel.

4. Conclusions

In this study $La_{0.6}Ca_{0.4}MnO_3$ powders were synthesized using the usual and modified citrate precursor methods. The effects of experimental variables on the formation of homogenous nano-sized powder with a pure perovskite structure were investigated using TG/DTA, IR, XRD, SEM, and BET. By using a modified citrate precursor method the calcination temperature can be reduced significantly, suggesting that La, Ca, and Mn were more uniformly dispersed in the $La_{0.6}Ca_{0.4}MnO_3$. The minimum temperature and time to obtain a single perovskite phase were 520˚C (<700˚C for the usual citrate method) and 2 h (<4 h for the usual citrate method). The $La_{0.6}Ca_{0.4}MnO_3$ powder specific surface area was 40.7 $m^2\ g^{-1}$, about 4-fold larger than that of the powder obtained from the usual citrate method.

References

[1] R.J.H. Voorhoeve, J.P. Remeika, L.E. Trimble, P.K. Gallagher, J. Sol. State. Chem. 14, 395 (1975)

[2] Y. Teraoka, T. Harada, H. Furukawa, S. Kagawa, in: L. Guczi (Ed.), New Frontiers in Catalysis, Proceedings of the 10th International Congress on Catalysis, 19-24 July 1992, Budapest, Hungary (Elsevier, Amsterdam, 1993) 2649

[3] J.L.G. Fierro, L.G. Tejuca, In: J.L.G. Fierro (Ed.), Properties and Applications of Perovskite-Type Oxides (Marcel Dekker, New York, 1993)

[4] K.S. Chan, J. Ma, S. Jaenicke, G.K. Chuah, J.Y. Lee, Appl. Catal. A: Gen. 107, 201 (1994)

[5] A.K. Ladavos, P.J. Pomonis, Appl. Catal. A: Gen. 165, 73 (1997)

[6] D. Ferri, L. Forni, M.A.P. Dekkers, B.E. Nieuwenhuys, Appl.Catal. B: Environ. 16, 339 (1998)

[7] Y. Yokoi, H. Uchida, Catal. Today 42, 167 (1998)

[8] R. Schneider, D. Kiessling, G. Wendt, W. Burckhardt, G.Winterstein, Catal. Today 47, 429 (1999)

[9] K.S. Song, H.X. Cui, S.D. Kim, S.K. Kang, Catal. Today 47, 155 (1999)

[10] R.E. Carbonio, C. Fierro, D. Tryk, D. Scherson, J. Power Sources 22, 387 (1988)

[11] V. Hermann, D. Dutriat, S. Muller, Ch. Comninellis, Electrochim. Acta 46, 365 (2000)

[12] X. Wang, P.J. Sebastian, M.A. Smit, H. Yang, S.A. Gamboab, J. Power Sources 124, 278 (2003)

[13] L. Jorissen, J. Power Sources 155, 23 (2006)

[14] T. Seiyama, Catal. Rev.-Sci. Eng. 34, 281 (1992)

[15] N. Yamazoe, Y. Teraoka, Catal. Today 8, 175 (1990)
[16] J. Kirchnerova, D. Kwana, J. Vaillancourt, J. Chaouki, Catal. Lett. 21, 77 (1993)
[17] J.M.D. Tascon, S. Mendioroz, T. Gonzalez, J. Phys. Chem. 14, 109 (1981)
[18] X. Li, H. Zhang, X. Liu, S. Li, M. Zhao, Mater. Chem. Phys. 38, 355 (1994)
[19] N.A. Merino, B.P. Barbero, P. Grange, L.E. Cadus, J. Catal. 231, 232 (2005)
[20] P. Courty, H. Ajot, C. Marcilly, B. Delmon, Power Technol. 7, 21 (1973)
[21] H.P. Klug, L.E. Alexander, X-ray Diffraction Procedures for Polycrystalline and Amorphous Materials (Wiley, London, 1962) 491
[22] S. Brunauer, P.H. Emmett, E. Teller, J. Am. Chem. Soc. 66, 309 (1938)
[23] M. Chaollang, D. Xianlin, Z. Tao, Mater. Lett. 61, 1633 (2007)
[24] Sh. Liu, X. Tan, K. Li, R. Hughes, Ceram. Int. 28, 327 (2002)
[25] X. Wang, Q. Cui, Y. Pan, G. Zou, J. Alloys Compd. 354, 91 (2003)
[26] F. Gao, R.A. Lewis, X.L. Wang, S.X. Dou, Physica C 2235, 341 (2000)
[27] X. Pingbo, Z. Wieping, Y. Kuo, J. Long, Z. Wiewei, X. Shangda, J. Alloys Compd. 311, 90 (2000)
[28] F. Gao, R.A. Lewis, X.L. Wang, S.X. Dou, J. Alloys Compd. 347, 314 (2002)
[29] G.Z. Chen, Ph.D. thesis, National Chen-Kung University (Taiwan, ROC, 2001)